Nanoscale Advances

ROYAL SOCIETY OF CHEMISTRY

PAPER

View Article Online
View Journal | View Issue

Cite this: *Nanoscale Adv.*, 2026, **8**, 1725

Magnetic resorcinol-formaldehyde supported Schiff-base/Cu as a robust and recoverable nanocatalyst for the synthesis of tetrahydrobenzo [*b*]pyrans

Parivash Bazmayon, Dawood Elhamifar * and Shiva Kargar

In this study, the design and synthesis of a magnetic resorcinol-formaldehyde (RF) functionalized with Schiff-base/Cu (Mag@RF/SB-Cu) nanocomposite are reported. The Mag@RF/SB nanomaterial was synthesized through the functionalization of the Mag@RF composite with (3-aminopropyl) trimethoxysilane, followed by the formation of a Schiff base *via* condensation with 2-hydroxybenzaldehyde. The resulting nanomaterial was subsequently treated with $Cu(NO_3)_2 \cdot 3H_2O$ to afford the Mag@RF/SB-Cu nanocomposite. The results obtained from FT-IR, EDX, PXRD, VSM and SEM analyses clearly confirmed the successful functionalization of the magnetite surface with the RF/SB-Cu complex, while retaining its crystalline structure. The Mag@RF/SB-Cu nanocomposite was used as a robust and efficient nanocatalyst for the synthesis of tetrahydrobenzo[*b*]pyrans in water at 25 °C. Using 0.005 g of the catalyst, the reactions gave the desired products in high yields (83–97%) within short times (15–35 min). Moreover, due to its good magnetic properties (24 emu per g), the catalyst exhibited remarkable reusability, retaining its catalytic performance over at least eight consecutive reaction cycles. The leaching test confirmed the heterogeneous nature of the Mag@RF/SB-Cu catalyst.

Received 13th July 2025
Accepted 13th January 2026

DOI: 10.1039/d5na00678c

rsc.li/nanoscale-advances

1 Introduction

In recent decades, heterogeneous catalysts have made significant advances as a result of their superior compatibility, improved efficiency, and simplicity of recycling, which have been driven by environmental concerns.[1–7] In this regard, nanoparticles (NPs) have attracted considerable attention due to their unique physicochemical properties, including high surface area, tunable morphology, and remarkable stability. These features also provide outstanding catalytic activity to NPs, allowing their efficient and sustainable application in a wide range of organic transformations.[8–11] Among various nanoparticles, magnetic core–shell structured nanocomposites, owing to their high surface area, exceptional thermomechanical stability, facile recovery, cost-effectiveness, and biocompatibility have garnered significant interest for the immobilization of homogeneous catalysts.[12–18] Moreover, these nanocomposites have been widely utilized in many applications such as gas storage[19,20] and separation,[21,22] water purification,[23–25] sensing,[26,27] photocatalysis[28,29] and drug delivery.[30,31] Various shell materials, including silica,[32,33] polymers,[34,35] inert metals[36,37] and carbon[38,39] can be employed to coat magnetic nanoparticles (MNPs) to form core–shell structured nanocomposites with high chemical stability and inhibit their assembly and aggregation. Resorcinol-formaldehyde (RF) resin has garnered increasing attention among various shell materials due to its unique physicochemical properties. The hydrophobic inner framework and phenolic hydroxyl-rich surface of RF facilitate the accumulation of reactants in proximity to catalytically active sites.[40,41] In addition, RF resin is appreciated for its biocompatibility, low toxicity, and cost-effectiveness, making it a promising candidate for catalytic applications.[42,43] Accordingly, MNPs coated with an RF shell can offer multiple advantages, including improved chemical stability, prevention of aggregation, and the favorable hydrophobic and biocompatible properties of the RF matrix. Nevertheless, despite these notable advantages, the catalytic application of RF-coated magnetic nanomaterials in multi-component organic transformations has remained largely underexplored. Some of these studies are Fe_3O_4@RF/Cu_2O,[44] CNTs@Fe_3O_4@RF,[45] Fe_3O_4@RF-Ag,[46] CNT-*g*-PDMAEMA/Fe_3O_4NPs[47] and MMS@IL/Cu.[48]

Meanwhile, Schiff-base ligands have attracted considerable interest in the fields of chemistry and materials science due to their effective complexation with diverse transition metal ions and outstanding catalytic efficacy. Moreover,

Department of Chemistry, Yasouj University, Yasouj, 75918-74831, Iran. E-mail: d.elhamifar@yu.ac.ir

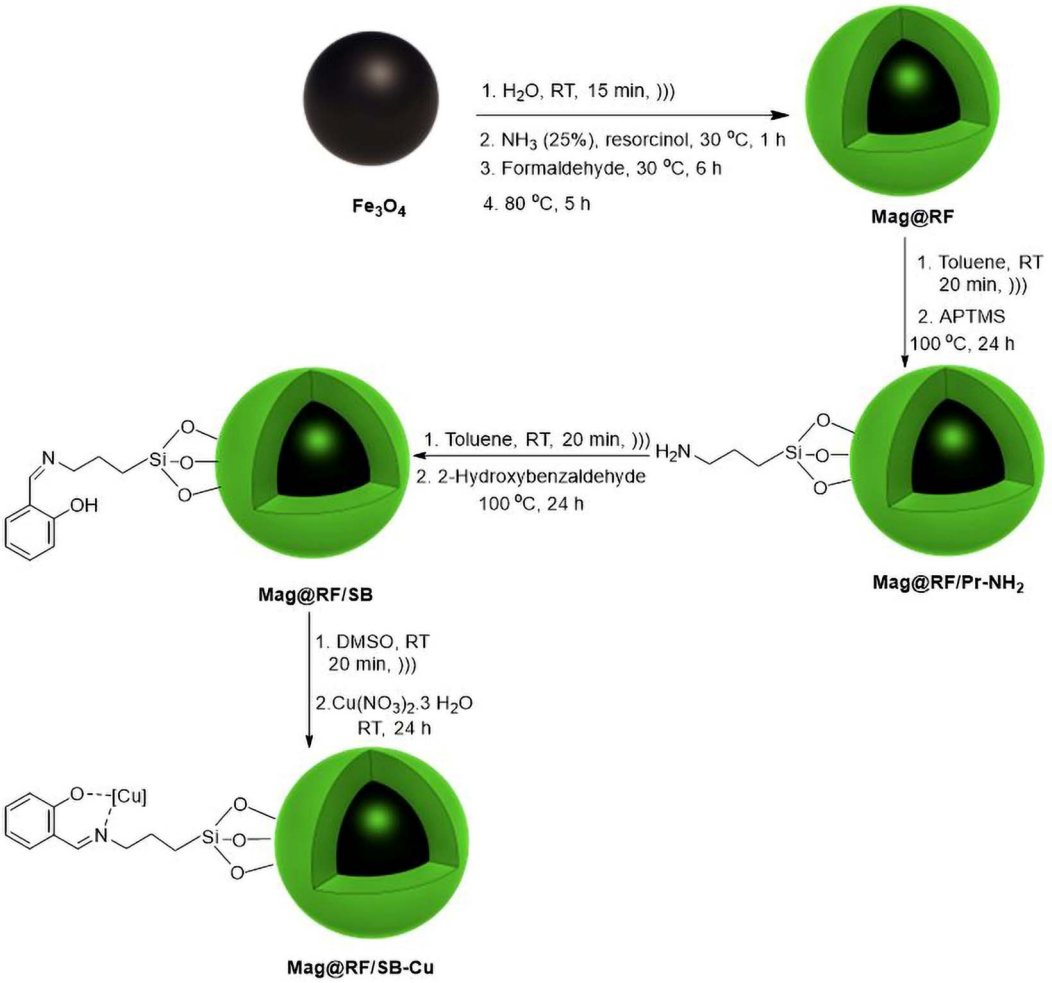

Scheme 1 Preparation of Mag@RF/SB-Cu.

Schiff-base ligands enhance the stability of catalysts *via* anchoring catalytic centers onto solid supports.[49–56] Some recent reports in this regard are copper-Schiff base@MCM-41,[57] Cu(II)[Sal(PMeOSi)DETA],[58] La-Schiff base@MCM-41 (ref. 59) and Fe_3O_4@SB@Cu.[60]

Multicomponent reactions (MCRs) have recently attracted considerable attention owing to their operational simplicity, excellent atom economy, and high synthetic efficiency. These features have positioned MCRs as a versatile and powerful strategy in modern organic synthesis and drug discovery.[61–64] Tetrahydrobenzo[*b*]pyrans represent a crucial class of compounds, serving as the core scaffold in numerous biologically active pharmaceuticals and are commonly synthesized *via* MCRs. These compounds display a broad spectrum of pharmacological activities, including anticonvulsant, antimicrobial, antiviral, antibacterial, anticancer, anticoagulant, anti-inflammatory and antifungal effects.[65–67] To date, numerous methods have been reported for the synthesis of tetrahydrobenzo[*b*]pyran derivatives.[68–70] However, the most of them suffer from disadvantages, including challenging product and catalyst separation, low yields and the utilization of hazardous solvents. Therefore, the challenge lies in finding a simple, highly efficient, fast, environmentally friendly and cost-efficient method to synthesize these compounds.

Considering the aforementioned, the present study introduces a magnetically separable and environmentally benign nanocatalyst comprising a resorcinol-formaldehyde-coated Fe_3O_4 core, functionalized with a Schiff-base-copper complex (Mag@RF/SB-Cu). To the best of our knowledge, this is the first report of such a hybrid nanostructure being designed and employed specifically for the one-pot synthesis of tetrahydrobenzo[*b*]pyran derivatives *via* MCRs. The novelty of this work lies in the synergistic integration of the highly dispersible and chemically stable RF shell with a robust Cu-Schiff-base complex, anchored on a magnetic support. This architecture combines magnetic recoverability, catalytic efficiency and stability, and biocompatibility, offering a promising pathway toward green and reusable heterogeneous catalysts in synthetic organic chemistry.

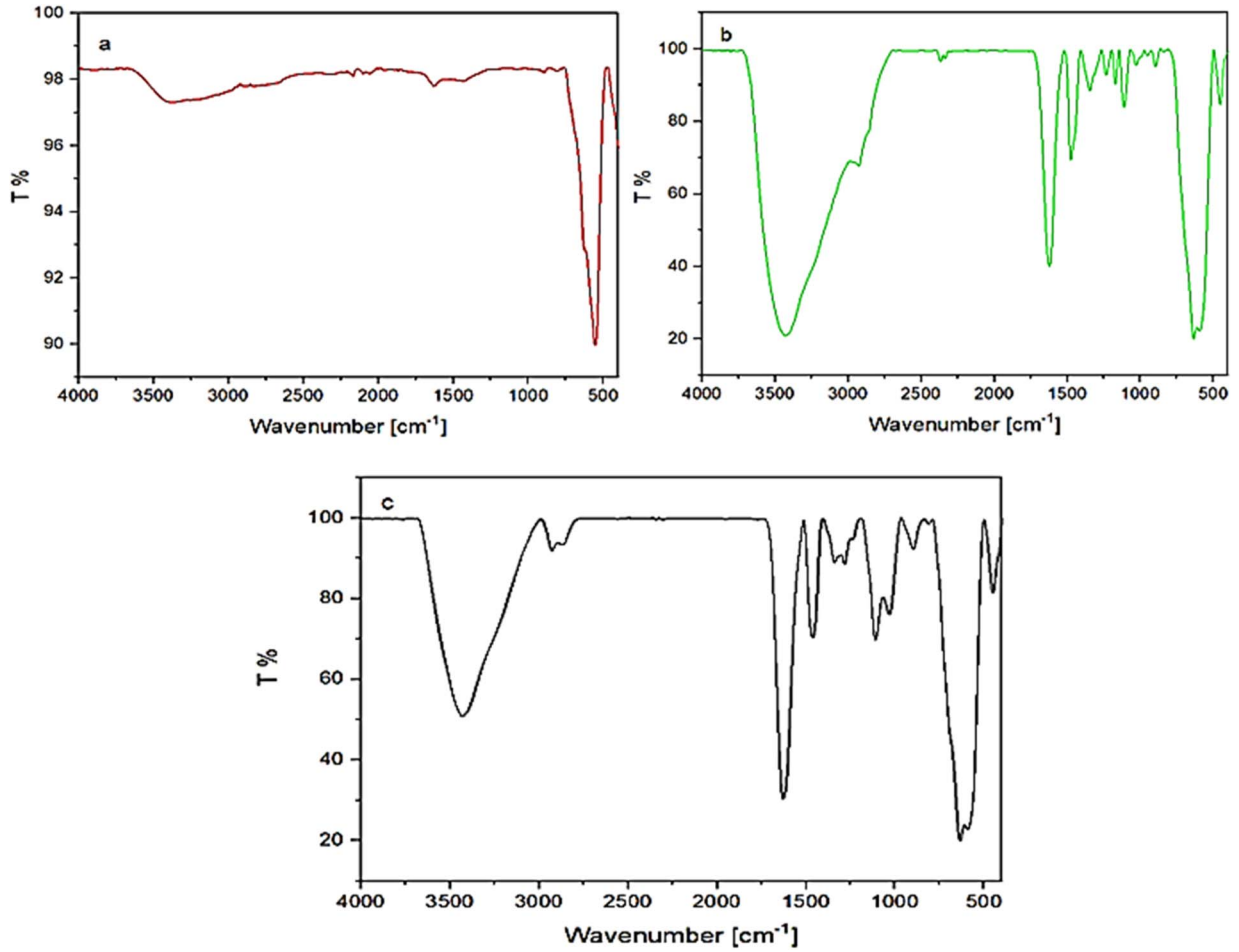

Fig. 1 FT-IR spectra of Fe_3O_4 (a), Mag@RF (b) and Mag@RF/SB-Cu (c).

2 Experimental section

2.1 General

All chemicals and reagents such as iron(II) chloride tetrahydrate (99%), iron(III) chloride hexahydrate (99%), ammonia (25% wt), resorcinol (≥99%), formaldehyde (37% wt), (3-aminopropyl)trimethoxysilane (97%), $Cu(NO_3)_2 \cdot 3H_2O$, dimedone (95%), malononitrile (≥99%), benzaldehydes (97–99%) were purchased from Fluka, Merck and Sigma-Aldrich. Fourier transform infrared (FT-IR) spectroscopy was performed on a Bruker-Vector 22 spectrometer (Germany). Powder X-ray diffraction (PXRD) patterns were obtained using a Rigaku Ultima IV diffractometer (Japan). Thermal gravimetric analysis (TGA) was performed using a Netzsch STA 409 PC/PG apparatus (Germany). Magnetic properties of the particles were measured using a vibrating sample magnetometer (VSM) by Meghnatis Daghigh Kavir Co. (Iran). The morphology of the particles was examined by using a ZEISS Sigma 300 field emission scanning electron microscope (FESEM, Germany). Energy dispersive X-ray (EDX) spectroscopy was performed by using a ZEISS Sigma 300 apparatus (Germany). Ultrasonication was carried out using an Elmasonic P60H ultrasonic bath (Elma, Germany).

2.2 Synthesis of Mag@RF

For this, the Fe_3O_4 NPs were initially synthesized following the procedure described in our previous work.[71] Subsequently, 1 g of the obtained Fe_3O_4 NPs were dispersed in 150 mL of water and sonicated for 15 min. After ultrasonic treatment, 0.3 mL of ammonia solution (25 wt%) and 0.4 g of resorcinol were added to the suspension and stirred at 30 °C for 1 h. Then, 0.6 mL of formaldehyde was added dropwise, and the mixture was continuously stirred for 6 h. The reaction mixture was then heated at 80 °C for 5 h to complete the polymerization. The resulting magnetic composite was collected using a magnet, thoroughly washed with EtOH and water, and dried at 70 °C for 6 h.[72] The product was named Mag@RF.

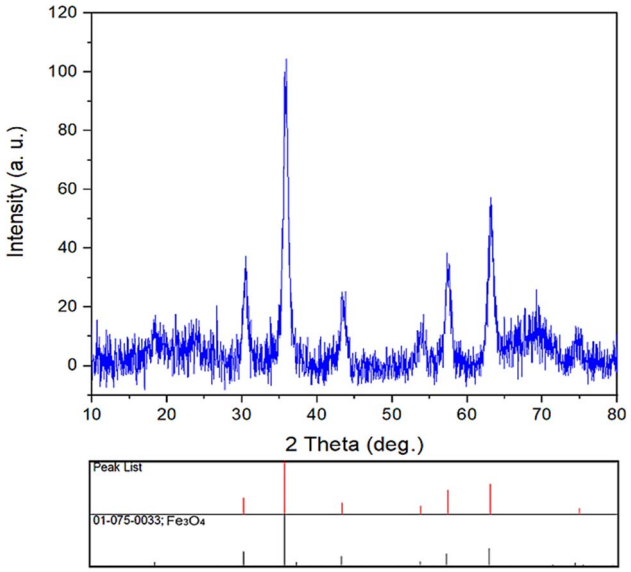

Fig. 2 PXRD pattern of Mag@RF/SB-Cu.

2.3 Synthesis of Mag@RF/Pr-NH_2

To functionalize the surface, 1 g of Mag@RF NPs was dispersed in 40 mL of toluene and sonicated at 25 °C for 20 min. Subsequently, 0.26 g of (3-aminopropyl)trimethoxysilane (APTMS) was added, and the mixture was stirred and refluxed at 100 °C for 24 h. The resulting magnetic solid was then separated using a magnet, thoroughly washed with EtOH and water, and dried at 70 °C for 6 h. The product was named Mag@RF/Pr-NH_2.

2.4 Synthesis of Mag@RF/SB

In this step, 1 g of Mag@RF/Pr-NH_2 was thoroughly dispersed in 40 mL of toluene and sonicated for 20 min. Then, 3 mL of 2-hydroxybenzaldehyde was added to the reaction vessel, and the mixture was heated at 100 °C under continuous stirring for 24 h. The resulting solid was collected by magnetic separation, washed repeatedly with EtOH and water, and dried in an oven at 70 °C for 6 h. The product was named Mag@RF/SB.

2.5 Synthesis of Mag@RF/SB-Cu

For this, initially, 1 g of Mag@RF/SB was thoroughly dispersed in 20 mL of DMSO and sonicated at 25 °C for 20 min. Subsequently, 2 mmol of copper(II) nitrate trihydrate was added, and the reaction mixture was stirred at 25 °C for 24 h. The resulting material was collected using a magnet, washed thoroughly with EtOH and water, and dried at 70 °C for 7 h. The product was named Mag@RF/SB-Cu.

2.6 Procedure for the preparation of tetrahydrobenzo[*b*]pyrans using Mag@RF/SB-Cu

For this, a mixture of aldehyde (1 mmol), malononitrile (1.3 mmol), dimedone (1 mmol) and Mag@RF/SB-Cu (0.005 g) was stirred in 10 mL of H_2O at 25 °C. The reaction progress was monitored by TLC. Upon completion, the catalyst was magnetically separated, and the resulting crude product was purified by recrystallization from EtOH to afford the pure compound.

3 Results and discussion

3.1 Characterization of Mag@RF/SB-Cu

Scheme 1 presents the stepwise synthesis of the Mag@RF/SB-Cu nanocomposite. Initially, magnetite NPs were encapsulated within a RF polymer matrix *via* interfacial polymerization under alkaline conditions. The resulting Mag@RF structure was subsequently modified with APTMS to introduce primary amine functionalities, affording Mag@RF/Pr-NH_2. This amine-functionalized material was then reacted with 2-hydroxybenzaldehyde to form Mag@RF/SB. Finally, coordination of copper(II) nitrate to the imine sites afforded the Mag@RF/SB-Cu nanocatalyst.

The stepwise functionalization of magnetite-based nanocomposites was monitored by FT-IR spectroscopy as depicted in Fig. 1. The pristine Fe_3O_4 NPs exhibited a characteristic Fe–O stretching band at 580 cm^{-1}, alongside a broad O–H stretching vibration centered at 3419 cm^{-1}, which remained present across all synthesized samples (Fig. 1a–c).[71] Following the deposition of the RF shell, new absorption bands appeared at 2860–2934 (CH_2 stretching), 1636 cm^{-1} (aromatic C=C stretching) and at 1088 and 1110 cm^{-1}, which are attributed to C–O–C stretching vibrations of methylene ether linkages within the RF network, confirming successful polymer coating (Fig. 1b and c).[41] Notably, the successful grafting of APTMS on the surface was confirmed by the stretching vibrations of Si–O bands appearing at 1077 and 925 cm^{-1} (Fig. 1b and c).[41,73] It should be noted that the imine (C=N) stretching vibration arising from Schiff-base formation appears near 1640–1650 cm^{-1}. However, in this system the C=N band overlaps with the aromatic C=C vibration of the RF network, resulting in a combined absorption near 1636–1645 cm^{-1} rather than a fully separated peak (Fig. 1c).[74] The preserved Fe–O absorption band and minimal changes in the RF signals confirm the structural stability of the material framework throughout synthesis of Mag@RF/SB-Cu.

Powder X-ray diffraction (PXRD) analysis was employed to investigate the crystalline structure of the Mag@RF/SB-Cu nanocomposite. As illustrated in Fig. 2, the diffraction pattern displays seven well-defined peaks at 2θ angles of 30.25°, 35.79°, 43.41°, 53.87°, 57.33°, 63.11° and 74.20°, which correspond to the (220), (311), (400), (422), (511), (440) and (533) planes characteristic of the spinel-type Fe_3O_4.[75] The high degree of correlation between these peaks and those observed for Fe_3O_4 clearly indicates that the crystalline nature of the magnetic core is retained throughout the surface modification and complexation processes, confirming its structural robustness.[76,77] Fig. 3 illustrates the EDX analysis of the Mag@RF/SB-Cu catalyst. This spectrum

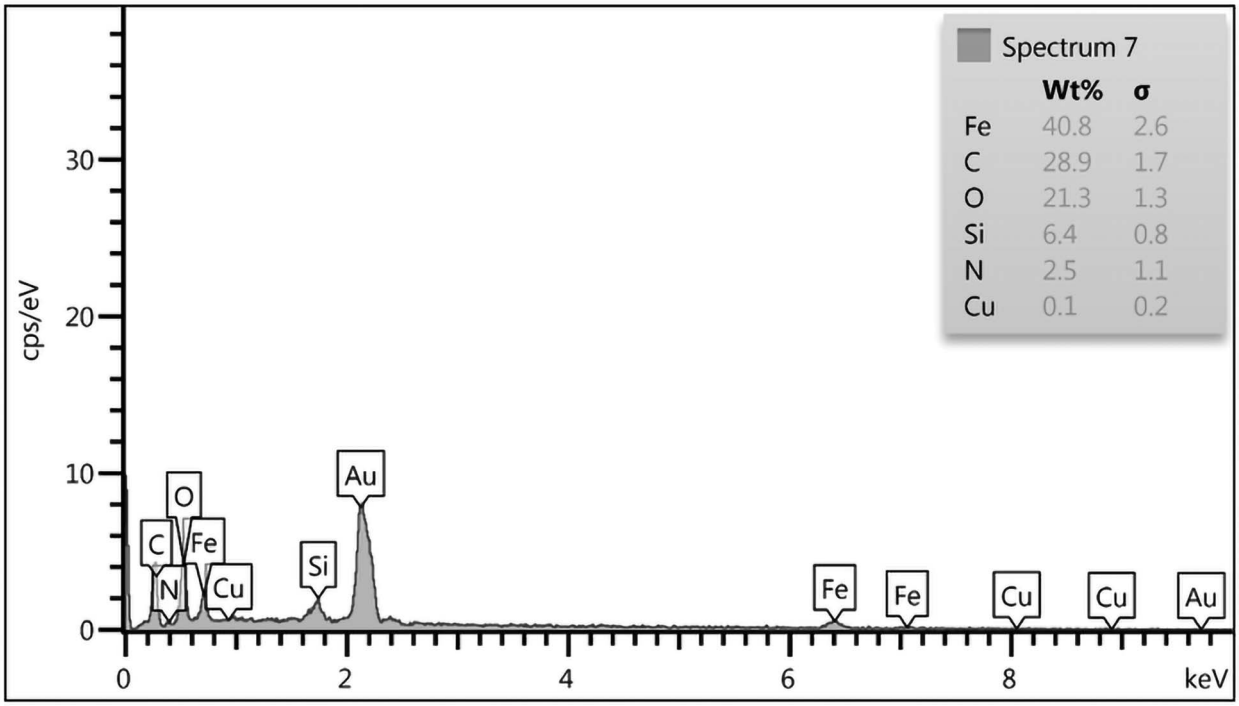

Fig. 3 EDX spectrum of Mag@RF/SB-Cu.

verifies the existence of Fe, C, O, Si, N and Cu elements in the designed material. This outcome aligns with the FTIR measurement, which proves the effective incorporation and immobilization of the expected species in the nanocomposite.

In addition, the EDX-mapping analysis (Fig. 4) showed that the predicted elements are distributed uniformly in the Mag@RF/SB-Cu framework, which is in agreement with the FT-IR and EDX results.

The thermal stability of the Mag@RF/SB-Cu composite was evaluated using thermogravimetric analysis (TGA) as shown in Fig. 5. An initial weight loss of approximately 3% occurred below 150 °C, which is attributed to the removal of adsorbed water. A major weight loss of ~38% between 200

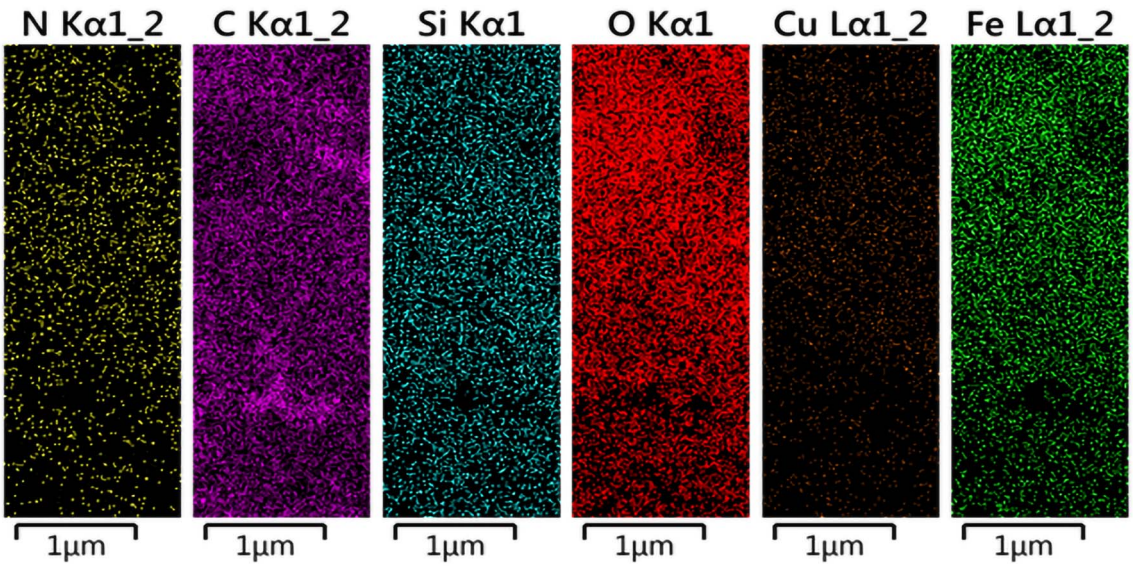

Fig. 4 EDX mapping of Mag@RF/SB-Cu.

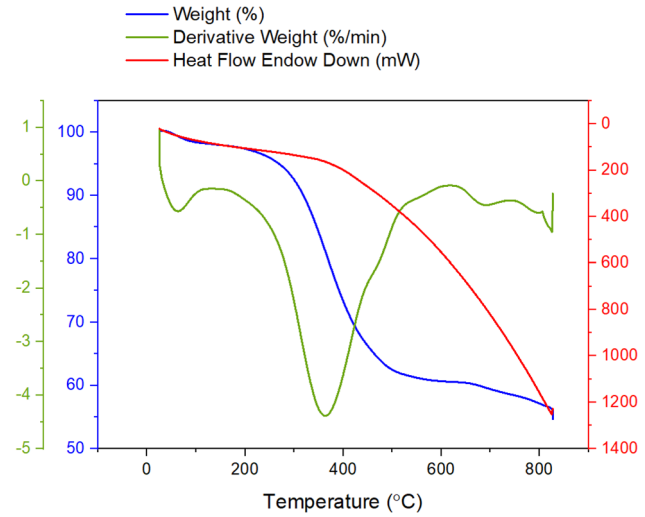

Fig. 5 TG curve of Mag@RF/SB-Cu.

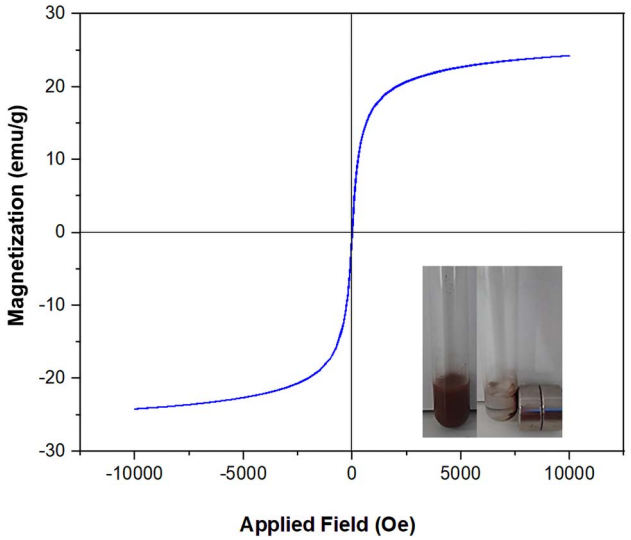

Fig. 6 VSM diagram of Mag@RF/SB-Cu.

and 500 °C is associated with the thermal decomposition of the RF polymer and organic Schiff base ligands. An additional weight loss of about 3% between 550 and 800 °C is due to the carbonization of residual organic components. These results prove that the designed composite exhibits good thermal stability, making it suitable for applications at elevated temperatures.

The magnetic properties of the Mag@RF/SB-Cu nanocomposite were evaluated using vibrating sample magnetometry (VSM), as depicted in Fig. 6. The material exhibited a saturation magnetization value of 24 emu per g. Notably, the absence of coercivity ($H_c = 0$) confirms the superparamagnetic nature of the Mag@RF/SB-Cu nanocomposite. Furthermore, the inset image in Fig. 6 demonstrates that the designed material can be efficiently separated from the solution through the application of an external magnetic field, highlighting its suitability for magnetic recovery and reuse in the catalytic processes.

Scanning electron microscopy (SEM) analysis was utilized to investigate the shape and distribution of the catalyst particles (Fig. 7). This analysis demonstrated that Mag@RF/SB-Cu possesses spherical particles with uniform dispersion.

3.2 Catalytic activity of Mag@RF/SB-Cu

Following successful characterization, the efficacy of the Mag@RF/SB-Cu catalyst was examined in the synthesis of tetrahydrobenzo[*b*]pyrans. The reaction between benzaldehyde, malononitrile and dimedone was used as a model to optimize the conditions. The effects of a variety of parameters, such as the amount of the catalyst and solvent were examined in order to determine the optimal conditions (Table 1). Notably, among the tested solvents (H_2O, EtOH and EtOH : H_2O) and solvent-free conditions, H_2O provided the highest catalytic performance, highlighting its potential as an efficient and environmentally benign medium (Table 1, entries 1–4). The amount of the catalyst was found to

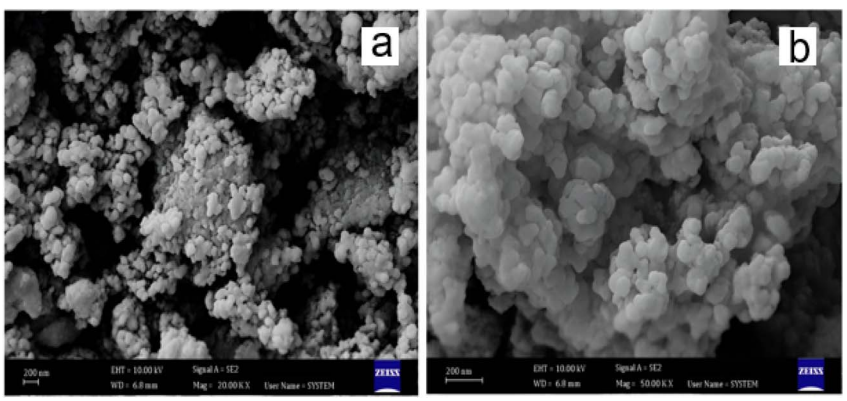

Fig. 7 SEM images of Mag@RF/SB-Cu at (a) low magnification and (b) high magnification.

Table 1 Optimization of the reaction conditions in the synthesis of tetrahydrobenzo[*b*]pyrans

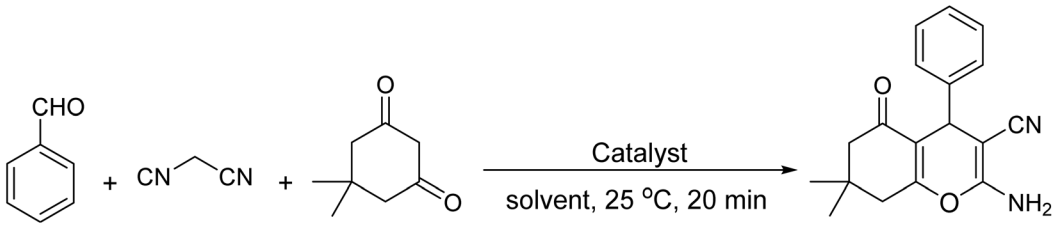

Entry	Catalyst	Solvent	Catalyst (g)	Yield[a] (%)
1	Mag@RF/SB-Cu	EtOH	0.005	82
2[b]	Mag@RF/SB-Cu	H_2O	0.005	95
3	Mag@RF/SB-Cu	EtOH/H_2O	0.005	85
4	Mag@RF/SB-Cu	Solvent-free	0.005	79
5	Mag@RF/SB-Cu	H_2O	0.008	95
6	Mag@RF/SB-Cu	H_2O	0.0025	63
7	—	H_2O	—	—
8	Mag@RF/SB	H_2O	0.005	—
9	Mag@RF	H_2O	0.005	—

[a] Isolated yields. [b] Optimal conditions.

significantly influence the reaction outcome. The optimal yield was achieved using 0.005 g of Mag@RF/SB-Cu (Table 1, entry 2). Increasing the catalyst loading to 0.008 g did not result in a noticeable improvement in yield (Table 1, entry 2 *vs.* entry 5). Importantly, no product formation was observed in the absence of Mag@RF/SB-Cu, confirming the essential role of the catalyst in this reaction (Table 1, entry 7). To clarify the specific role of Cu centers in the catalytic activity, a control experiment was carried out using Cu-free Mag@RF-SB and Mag@RF materials under the same reaction conditions (Table 1, entries 8 and 9). The results indicated that, in the absence of Cu species, no product was formed, highlighting the essential role of copper sites in facilitating the catalytic process.

With the optimized conditions in hand, a range of aromatic aldehydes featuring either electron-donating or electron-withdrawing groups were subjected to the reaction. In all cases, the corresponding tetrahydrobenzo[*b*]pyran derivatives were obtained in high to excellent yields, highlighting the robustness and versatility of the Mag@RF/SB-Cu catalyst (Table 2). The precision of the described method under the optimized conditions using Mag@RF/SB-Cu was evaluated through four replicate runs for all reactions. The relative standard deviation (RSD) was found to be between 1.3 and 2.3%, indicating high reproducibility of the method.

Given the critical role of catalyst stability in practical applications, the recoverability and reusability of the Mag@RF/SB-Cu catalyst were investigated. After each reaction cycle, the catalyst was magnetically recovered and reused under optimized conditions. Remarkably, the designed catalyst retained its catalytic efficiency for at least eight consecutive runs, highlighting its excellent stability and durability under the applied conditions (Fig. 8).

To investigate the chemical and structural stability of the Mag@RF/SB-Cu nanocatalyst, the recovered catalyst was characterized using FT-IR, PXRD and SEM analyses. As illustrated in Fig. 9, the FT-IR spectra of the fresh and recycled catalyst after eight reaction cycles exhibited identical patterns without any significant changes in the characteristic absorption bands. These results demonstrate that the catalyst retained its structural integrity during repeated use.

Similarly, the PXRD pattern of the recovered catalyst (Fig. 10) remained unchanged compared with the fresh sample, indicating the high stability of the crystalline structure of Fe_3O_4 after consecutive recovery and reuse cycles.

Moreover, the SEM image of the recycled catalyst (Fig. 11) further confirmed that its morphology was preserved after eight catalytic runs. These results highlight the remarkable chemical stability and reusability of the Mag@RF/SB-Cu nanocatalyst.

To confirm the heterogeneous nature of the Mag@RF/SB-Cu catalyst, a leaching test was carried out under the optimized conditions. In this test, the catalyst was magnetically separated from the reaction mixture after approximately 50% conversion, and the remaining solution was stirred for an additional 60 min. No further progress in the reaction was observed, confirming the efficient immobilization and high stability of the Cu centers. This high stability is attributed to the strong coordination of Cu species with the Schiff-base

Table 2 Synthesis of tetrahydrobenzo[*b*]pyrans catalyzed by Mag@RF/SB-Cu

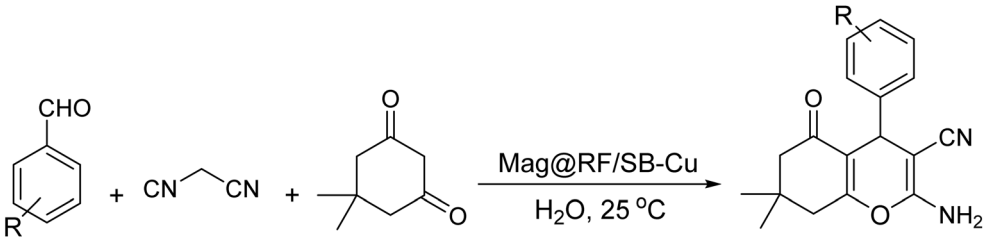

Entry	Aldehyde	Time (min)	Yield (%)	Found M. P. (°C)	Reported M. P. (°C)
1	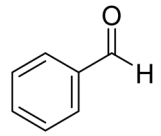	20	95 ± 1.3	228–230	229–231 (ref. 67)
2	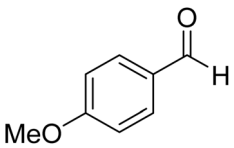	35	83 ± 1.5	198–200	199–201 (ref. 78)
3	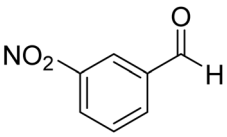	22	96 ± 2.2	208–210	211–212 (ref. 78)
4	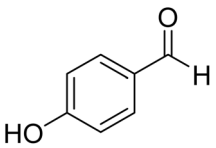	32	86 ± 2.3	204–206	205–207 (ref. 79)
5	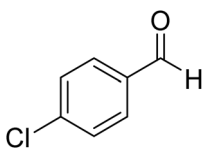	28	94 ± 1.7	208–210	210–212 (ref. 67)
6	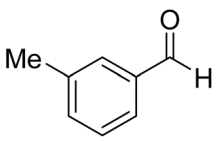	30	85 ± 2	203–205	206–208 (ref. 80)
7	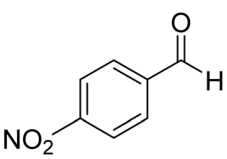	17	97 ± 1.8	182–184	179–181 (ref. 67)

ligands, which effectively prevents metal leaching during the reaction.

A plausible mechanism for the formation of tetrahydrobenzo [*b*]pyrans using the Mag@RF/SB-Cu catalyst is proposed in Scheme 2. Initially, 2-arylidene malononitrile (**1**) is generated *via* the Knoevenagel condensation of the Cu-activated aldehyde with malononitrile. Subsequently, a Michael-type addition between intermediate **1** and the enolized form of dimedone affords intermediate **2**. This intermediate then undergoes intramolecular cyclization to yield intermediate **3**, which finally undergoes tautomerization to deliver the desired product **4** in excellent yield.[81]

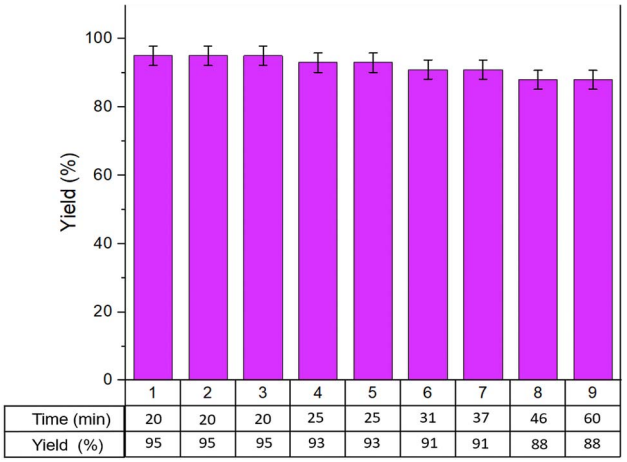

	1	2	3	4	5	6	7	8	9
Time (min)	20	20	20	25	25	31	37	46	60
Yield (%)	95	95	95	93	93	91	91	88	88

Fig. 8 Recoverability and reusability of Mag@RF/SB-Cu.

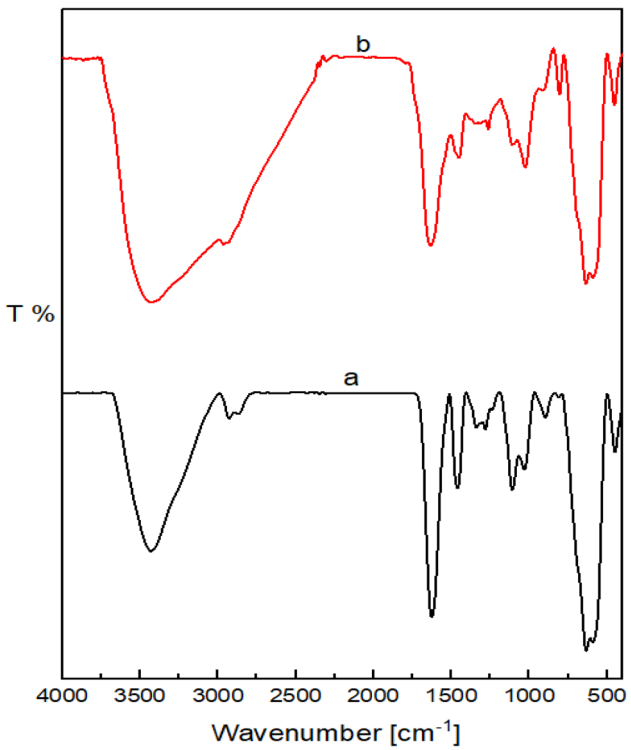

Fig. 9 FT-IR spectra of the fresh (a) and recovered Mag@RF/SB-Cu catalyst (b).

Finally, the efficiency of the Mag@RF/SB-Cu catalyst was compared with several previously reported catalysts for the synthesis of tetrahydrobenzo[*b*]pyran derivatives (Table 3). The results clearly demonstrated that Mag@RF/SB-Cu exhibits superior performance in terms of lower catalyst loading, lower temperature and higher recovery times. This remarkable efficiency is attributed to the magnetic character of the present catalyst, hydrophobic nature of RF resin and also the key role of Schiff-base ligands in the robust immobilization of Cu active sites.

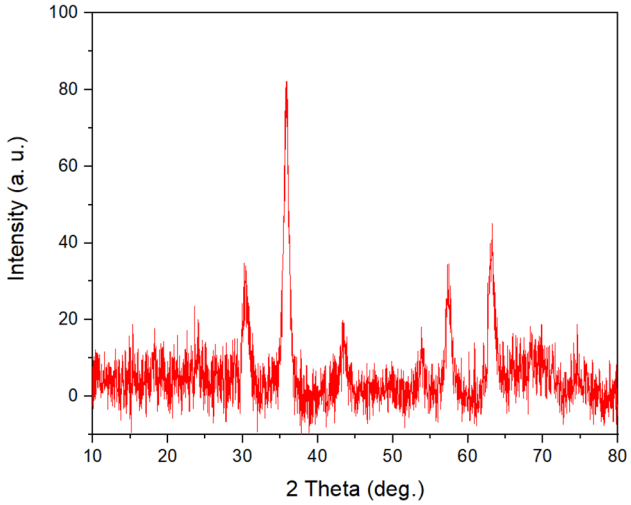

Fig. 10 PXRD pattern of the recovered Mag@RF/SB-Cu catalyst.

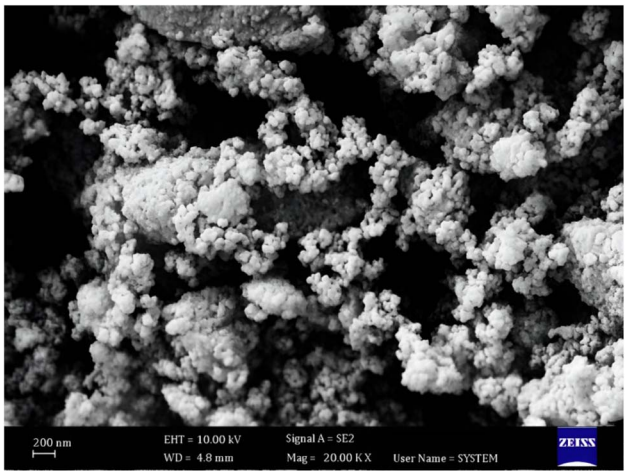

Fig. 11 SEM image of the recovered Mag@RF/SB-Cu nanocatalyst.

4 Conclusion

In summary, a novel resorcinol-formaldehyde-coated magnetite nanocomposite functionalized with a Schiff-base-Cu complex (Mag@RF/SB-Cu) was successfully synthesized. The effective immobilization of the SB-Cu complex on the Mag@RF surface was evidenced by the FT-IR, TG, and EDX measurements. The SEM analysis revealed a spherical structure for this designed nanomaterial. Moreover, the VSM analysis confirmed the superparamagnetic behavior of this nanocomposite. Mag@RF/SB-Cu was effectively applied as a powerful nanocatalyst for the green synthesis of tetrahydrobenzo[*b*]pyrans in water as an environmentally friendly solvent at room temperature. The developed catalyst was easily recovered and reused, and its efficiency and stability remained unchanged after recycling eight times. Due to the aforementioned advantages of the designed Mag@RF/SB-Cu catalyst, its application in other

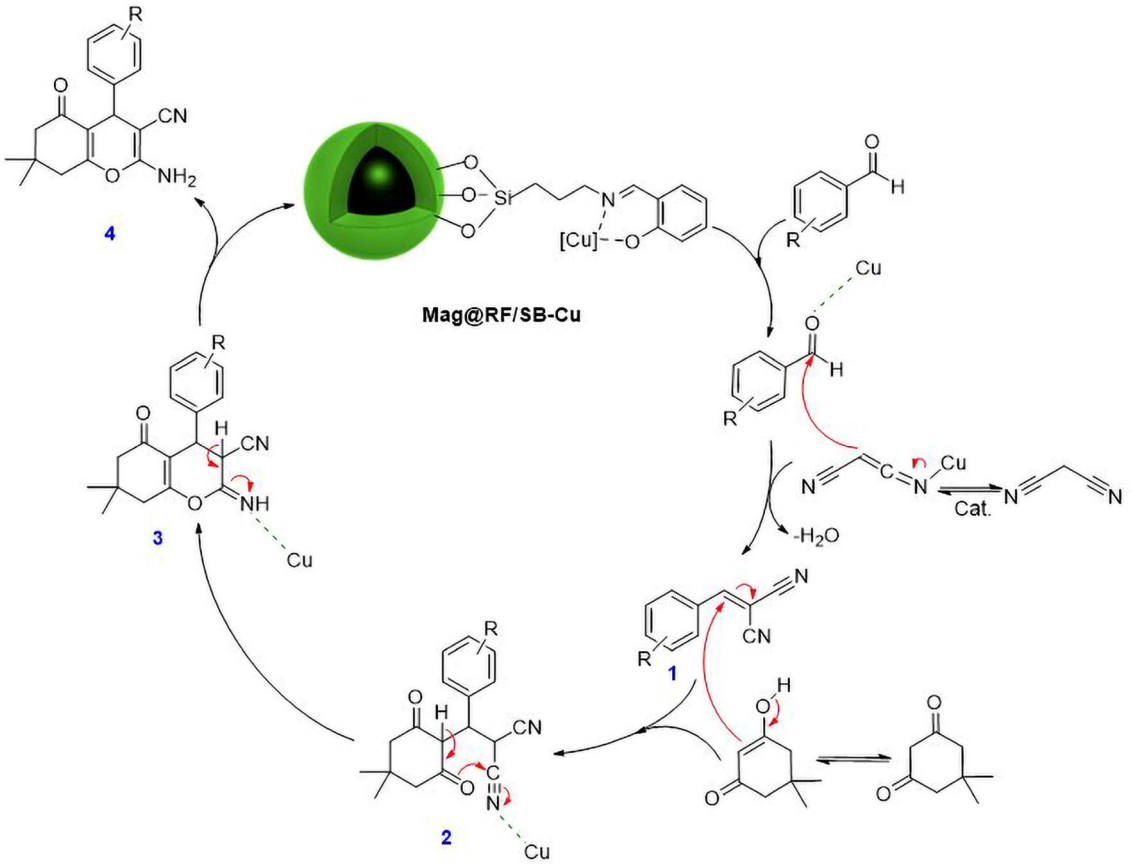

Scheme 2 A plausible mechanism for the synthesis of tetrahydrobenzo[*b*]pyrans using Mag@RF/SB-Cu.

Table 3 Comparative study of the efficiency of Mag@RF/SB-Cu with previously reported catalysts in the synthesis of tetrahydrobenzo[*b*]pyrans

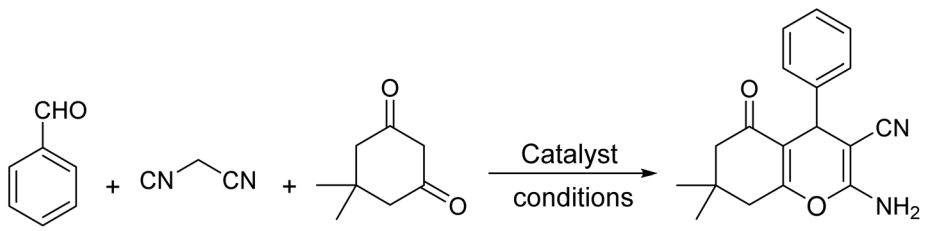

Entry	Catalyst	Conditions	Recovery times	References
1	Fe_3O_4@SiO_2@TiO_2	Cat. (0.01 g), solvent-free, 100 °C	6	82
2	H_2PO_4-SCMNPs	Cat. 0.03 g, solvent-free, 60 °C	5	83
3	GO–Si–NH_2–PMo	Cat. 0.04 g, solvent-free, 90 °C	5	84
4	Fe_3O_4@NFCs/E-CHDA-Cu^{II}	Cat. 0.005 g, solvent-free, 25 °C	4	85
5	Mag@RF/SB-Cu	Cat. 005 g, H_2O, 25 °C	8	This work

chemical transformations is currently under investigation in our laboratory.

Author contributions

P. B.: investigation, resources, formal analysis. D. E.: conceptualization, writing—review and editing, supervision, visualization. S. K. writing—original draft, formal analysis.

Conflicts of interest

There are no conflicts to declare.

Data availability

All raw and processed FT-IR, PXRD, VSM and TGA data supporting this article are provided in the supplementary information (SI). Supplementary information is available. See DOI: https://doi.org/10.1039/d5na00678c.

Acknowledgements

The authors acknowledge Yasouj University and Iran National Science Foundation (INSF) for supporting this work.

References

1 B. El Allaoui, H. Benzeid, N. Zari, A. el kacem Qaiss and R. Bouhfid, Cellulose beads supported CoFe2O4: a novel heterogeneous catalyst for efficient rhodamine B degradation via advanced oxidation processes, *Int. J. Biol. Macromol.*, 2024, **259**, 128893.
2 S. Guan, Y. Liu, H. Zhang, R. Shen, H. Wen, N. Kang, J. Zhou, B. Liu, Y. Fan and J. Jiang, Recent advances and perspectives on supported catalysts for heterogeneous hydrogen production from ammonia borane, *Adv. Sci.*, 2023, **10**, 2300726.
3 X. Yao, S. Yuan, C. Li, L. Wang, X. Yu, P. Tian and S.-t. Tu, ZnO-supported palladium catalysts via ball milling as an effective heterogeneous catalyst for methanol steam reforming, *Fuel*, 2024, **358**, 130133.
4 T. Pu, W. Zhang and M. Zhu, Engineering heterogeneous catalysis with strong metal–support interactions: characterization, theory and manipulation, *Angew. Chem., Int. Ed.*, 2023, **62**, e202212278.
5 M. Kohantorabi, G. Moussavi and S. Giannakis, A review of the innovations in metal-and carbon-based catalysts explored for heterogeneous peroxymonosulfate (PMS) activation, with focus on radical vs. non-radical degradation pathways of organic contaminants, *Chem. Eng. J.*, 2021, **411**, 127957.
6 A. A. Ibrahim, R. S. Salama, S. A. El-Hakam, A. S. Khder and A. I. Ahmed, Synthesis of sulfated zirconium supported MCM-41 composite with high-rate adsorption of methylene blue and excellent heterogeneous catalyst, *Colloids Surf., A*, 2021, **616**, 126361.
7 H. Xiang, B. Liang, Y. Zhang, S. Luo and F. Jing, Fabricating hollow silica microsphere-supported bimetallic nickel-copper catalyst to promote the vapor phase hydrogenation of levulinic acid to γ-valerolactone, *Colloids Surf., A*, 2025, **705**, 135559.
8 J. Ali, S. Bibi, W. B. Jatoi, M. Tuzen, M. A. Jakhrani, X. Feng and T. A. Saleh, Green synthesized zinc oxide nanostructures and their applications in dye-sensitized solar cells and photocatalysis: A review, *Mater. Today Commun.*, 2023, **36**, 106840.
9 S. Boher, R. Ullah, M. Tuzen and T. A. Saleh, Metal doped nanocomposites for detection of pesticides and phenolic compounds by colorimetry: Trends and challenges, *OpenNano*, 2023, **13**, 100168.
10 M. Yaseen, K. Khalid, S. Bibi, A. Khan, M. Tuzen and T. A. Saleh, Recent trends in Photoelectrocatalysts: Types, influencing factors, and versatile applications: A comprehensive review, *Sustainable Mater. Technol.*, 2024, **41**, e01067.
11 R. Ullah and M. Tuzen, Photocatalytic removal of organic dyes by titanium doped alumina nanocomposites: Using multivariate factorial and kinetics models, *J. Mol. Struct.*, 2023, **1285**, 135509.
12 W. Xie, C. Gao and J. Li, Sustainable biodiesel production from low-quantity oils utilizing H6PV3MoW8O40 supported on magnetic Fe3O4/ZIF-8 composites, *Renewable Energy*, 2021, **168**, 927–937.
13 W. Xie and H. Wang, Grafting copolymerization of dual acidic ionic liquid on core-shell structured magnetic silica: A magnetically recyclable Brönsted acid catalyst for biodiesel production by one-pot transformation of low-quality oils, *Fuel*, 2021, **283**, 118893.
14 N. Aflak, H. Ben El Ayouchia, L. Bahsis and S.-E. Stiriba, Copper (I) Supported on Fe3O4/Glycine Nanocomposite: A Sustainable Magnetic Nanocatalyst for Click Synthesis of 1, 2, 3-Triazoles in Water, *Catal. Lett.*, 2025, **155**, 162.
15 M. A. El-Aal, A. E.-A. A. Said, M. N. Goda, E. F. Abo Zeid and S. M. Ibrahim, Fe3O4@CMC-Cu magnetic nanocomposite as an efficient catalyst for reduction of toxic pollutants in water, *J. Mol. Liq.*, 2023, **385**, 122317.
16 R. Kore, A. D. Sawant and R. D. Rogers, Recyclable magnetic Fe3O4 nanoparticle-supported chloroaluminate ionic liquids for heterogeneous lewis acid catalysis, *ACS Sustain. Chem. Eng.*, 2021, **9**, 8797–8802.
17 X. Huang, Y. Niu, Z. Peng and W. Hu, Core–shell structured BiOCl@ polydopamine hierarchical hollow microsphere for highly efficient photocatalysis, *Colloids Surf., A*, 2019, **580**, 123747.
18 H. Zeng, L. Zhai, T. Qiao, J. Zhang and D. Li, Removal of As (V) by a core-shell magnetic nanoparticles synthesized with iron-containing water treatment residuals, *Colloids Surf., A*, 2021, **627**, 127074.
19 K. Wang, B.-L. Wang, Y. Li, X.-D. Wang, C.-H. Min and Z.-H. Rao, A numerical study on regulating the latent heat storage process of Fe3O4-paraffin wax composite materials by using gradient magnetic field, *Int. J. Heat Mass Transfer*, 2024, **231**, 125874.

20 Y. Wu, T. Tang, L. Shi and Y. He, Rapid hydrate-based methane storage promoted by bilayer surfactant-coated Fe3O4 nanoparticles under a magnetic field, *Fuel*, 2021, **303**, 121248.
21 R. Nithya, A. Thirunavukkarasu, A. B. Sathya and R. Sivashankar, Magnetic materials and magnetic separation of dyes from aqueous solutions: a review, *Environ. Chem. Lett.*, 2021, **19**, 1275–1294.
22 P. Cheng, C. Liu, S. Du, C. Xu, X. Han, T. Zhu and W. Liang, Magnetic separation and recovery of powder particles from water using Fe3O4@ CTS-BDAT, *Sep. Purif. Technol.*, 2025, **364**, 132528.
23 C. Wang, X. Liu, T. Yang, D. Sridhar, H. Algadi, B. B. Xu, Z. M. El-Bahy, H. Li, Y. Ma and T. Li, An overview of metal-organic frameworks and their magnetic composites for the removal of pollutants, *Sep. Purif. Technol.*, 2023, **320**, 124144.
24 Y. Peng, M. Azeem, R. Li, L. Xing, Y. Li, Y. Zhang, Z. Guo, Q. Wang, H. H. Ngo and G. Qu, Zirconium hydroxide nanoparticle encapsulated magnetic biochar composite derived from rice residue: application for As (III) and As (V) polluted water purification, *J. Hazard. Mater.*, 2022, **423**, 127081.
25 M. F. Lanjwani, M. Tuzen, M. Y. Khuhawar and T. A. Saleh, Trends in photocatalytic degradation of organic dye pollutants using nanoparticles: A review, *Inorg. Chem. Commun.*, 2024, **159**, 111613.
26 M. A. Khan, J. Sun, B. Li, A. Przybysz and J. Kosel, Magnetic sensors-A review and recent technologies, *Eng. Res. Express*, 2021, **3**, 022005.
27 M. Bichurin, R. Petrov, O. Sokolov, V. Leontiev, V. Kuts, D. Kiselev and Y. Wang, Magnetoelectric magnetic field sensors: A review, *Sensors*, 2021, **21**, 6232.
28 Y. Feng, X. Su, Y. Chen, Y. Liu, X. Zhao, C. Lu, Y. Ma, G. Lu and M. Ma, Research progress of graphene oxide-based magnetic composites in adsorption and photocatalytic degradation of pollutants: A review, *Mater. Res. Bull.*, 2023, **162**, 112207.
29 S. Cheng, S. Zhao, B. Xing, Y. Liu, C. Zhang and H. Xia, Preparation of magnetic adsorbent-photocatalyst composites for dye removal by synergistic effect of adsorption and photocatalysis, *J. Cleaner Prod.*, 2022, **348**, 131301.
30 X. Wang, Y. Qi, Z. Hu, L. Jiang, F. Pan, Z. Xiang, Z. Xiong, W. Jia, J. Hu and W. Lu, Fe3O4@ PVP@ DOX magnetic vortex hybrid nanostructures with magnetic-responsive heating and controlled drug delivery functions for precise medicine of cancers, *Adv. Compos. Hybrid Mater.*, 2022, **5**, 1786–1798.
31 A. Mohan, R. Suresh, M. Ashwini, G. Periyasami, L. Guganathan, M.-C. Lin, K. Kumarasamy, S.-C. Kim and M. Santhamoorthy, Alginate functionalized magnetic-silica composites for pH-responsive drug delivery and magnetic hyperthermia applications, *Mater. Lett.*, 2024, **361**, 136088.
32 A. Khalid, R. Ahmed, M. Taha and T. Soliman, Fe3O4 nanoparticles and Fe3O4@ SiO2 core-shell: synthesize, structural, morphological, linear, and nonlinear optical properties, *J. Alloys Compd.*, 2023, **947**, 169639.
33 Y. Hou, B. Li, J. Chen, X. Shen, B. Wang, K. Liu, S. Wei, X. He, D. Li and Q. Han, Electromagnetic wave absorption properties of core double-shell structured α-Fe (Si)@ Fe3O4@ SiO2 composites, *Appl. Surf. Sci.*, 2023, **615**, 156345.
34 W. Qin, R. Li, H. Li, G. Jiang, G. Qin, Y. Wang and J. Yang, A nano-Fe3O4 material coated with AM/AMPS copolymer for viscosity enhancement at harsh reservoir conditions, *J. Appl. Polym. Sci.*, 2021, **138**, 50601.
35 T. Zhang, X. Qu, S. Sun, Z. Zhang, Y. Qiu, P. Wu and P. Ding, Engineering Cu-Fe3O4/Polymer Dots Hybrids for Dual-Mode Detection of Chlortetracycline, Recognition-Enhanced Water Pollutant Degradation, and Bacterial Disinfection, *Small*, 2025, **21**, 2501187.
36 P. Miao, Y. Tang and L. Wang, DNA modified Fe3O4@ Au magnetic nanoparticles as selective probes for simultaneous detection of heavy metal ions, *ACS Appl. Mater. Interfaces*, 2017, **9**, 3940–3947.
37 Y. Tuo, G. Liu, B. Dong, J. Zhou, A. Wang, J. Wang, R. Jin, H. Lv, Z. Dou and W. Huang, Microbial synthesis of Pd/Fe3O4, Au/Fe3O4 and PdAu/Fe3O4 nanocomposites for catalytic reduction of nitroaromatic compounds, *Sci. Rep.*, 2015, **5**, 13515.
38 J. Guo, Y. Sun, X. Li, G. Zhao, M. H. Helal, D. Pan, H. K. Thabet, W. Wu, W. Abdul and S. M. El-Bahy, Carbonization Tuned Core-Shell Fe3O4@ C Nanostructures with Enhanced Electromagnetic Wave Absorption, *Adv. Mater. Interfaces*, 2025, 2500075.
39 P. He, W. Ma, J. Xu, Y. Wang, Z. K. Cui, J. Wei, P. Zuo, X. Liu and Q. Zhuang, Hierarchical and orderly surface conductive networks in yolk–shell Fe3O4@ C@ Co/N-doped C microspheres for enhanced microwave absorption, *Small*, 2023, **19**, 2302961.
40 C. Shi, C. Lin, X. Huang, Q. Wu, H. Ge and Y. Yang, Facile synthesis of magnetic resorcinol–formaldehyde resin Fe3O4@ RF-Au composites for enhanced tetracycline photodegradation with simultaneous H2O2 production, *J. Mater. Sci.:Mater. Electron.*, 2024, **35**, 1070.
41 P. Dehghani, D. Elhamifar and S. Kargar, Amine functionalized magnetic resorcinol formaldehyde as a green and reusable nanocatalyst for the Knoevenagel condensation, *Sci. Rep.*, 2025, **15**, 2873.
42 L. Yang, Y. Wang, T. Chen, L. Liu, Y. Cai, J. Fang and Y. Yang, Impact of varying the core–shell structural sequence on the efficiency of cascade reagent-free Fenton-like oxidation: the case of magnetically recycling resorcinol–formaldehyde resin/magnetite composite microspheres, *Dalton Trans.*, 2025, **54**, 5164–5181.
43 F. Kiani, D. Elhamifar and S. Kargar, Magnetic resorcinol–formaldehyde supported isatin-Schiff-base/Fe as a green and reusable nanocatalyst for the synthesis of pyrano[2,3-d]pyrimidines, *Nanoscale Adv.*, 2025, **7**, 1552–1560.
44 M. Wang, Y. Ni and A. Liu, Fe3O4@ resorcinol–formaldehyde resin/Cu2O composite microstructures: solution-phase construction, magnetic performance, and applications in antibacterial and catalytic fields, *ACS Omega*, 2017, **2**, 1505–1512.

45 D. Zheng, M. Zhang, L. Ding, Y. Zhang, J. Zheng and J. Xu, Facile synthesis of magnetic resorcinol–formaldehyde (RF) coated carbon nanotubes for methylene blue removal, *RSC Adv.*, 2016, **6**, 11973–11979.

46 Y. Zhong, Y. Ni, S. Li and M. Wang, Chain-like Fe3O4@resorcinol-formaldehyde resins–Ag composite microstructures: facile construction and applications in antibacterial and catalytic fields, *RSC Adv.*, 2016, **6**, 15831–15837.

47 L. Geng, Y. Tian, R. Ding, C. Zhao, W. Yang, Q. Shi and H. Xu, Magnetite nanoparticles immobilized on hydrophilic polyelectrolyte-grafted carbon nanotube as efficient organic–inorganic hybrid heterogeneous catalyst for Knoevenagel condensation in aqueous medium, *Colloids Surf., A*, 2024, **685**, 133283.

48 S. Kargar and D. Elhamifar, Magnetic Mesoporous Silica Nanocomposite Supported Ionic Liquid/Cu as a Powerful and Highly Stable Catalyst for Chan-Lam Coupling Reaction, *Silicon*, 2024, **16**, 5285–5299.

49 V. K. Juyal, A. Pathak, M. Panwar, S. C. Thakuri, O. Prakash, A. Agrwal and V. Nand, Schiff base metal complexes as a versatile catalyst: A review, *J. Organomet. Chem.*, 2023, **999**, 122825.

50 S. De, A. Jain and P. Barman, Recent advances in the catalytic applications of chiral schiff-base ligands and metal complexes in asymmetric organic transformations, *ChemistrySelect*, 2022, **7**, e202104334.

51 H. Zhang, P. Wang, W. Shan, Y. Xiong, Z. Xing and H. Yu, Synthesis of schiff base-functionalized ordered mesoporous silica for effective adsorption of Re (VII), *Colloids Surf., A*, 2024, **690**, 133792.

52 Y. Yang, Y. Zhang, S. Hao, J. Guan, H. Ding, F. Shang, P. Qiu and Q. Kan, Heterogenization of functionalized Cu(II) and VO(IV) Schiff base complexes by direct immobilization onto amino-modified SBA-15: Styrene oxidation catalysts with enhanced reactivity, *Appl. Catal., A*, 2010, **381**, 274–281.

53 S. N. Ghalebin, A. Bezaatpour, M. H. Sadr, M. S. Sadjadi, M. K. Moghaddam and S. Szunerits, [1+1] Copper(II) macrocyclic Schiff base complex on rGO as a photocatalyst for reduction of nitroaromatics compounds under visible-light irradiation, *J. Mol. Liq.*, 2021, **328**, 115338.

54 D. Majumdar, B. Gassoumi, A. Dey, S. Roy, S. Ayachi, S. Hazra and S. Dalai, Synthesis, characterization, crystal structure, and fabrication of photosensitive Schottky device of a binuclear Cu(ii)-Salen complex: a DFT investigations, *RSC Adv.*, 2024, **14**, 14992–15007.

55 D. Elhamifar, P. Mofatehnia and M. Faal, Magnetic nanoparticles supported Schiff-base/copper complex: An efficient nanocatalyst for preparation of biologically active 3, 4-dihydropyrimidinones, *J. Colloid Interface Sci.*, 2017, **504**, 268–275.

56 S. Rezayati, A. Ramazani, S. Sajjadifar, H. Aghahosseini and A. Rezaei, Design of a Schiff Base Complex of Copper Coated on Epoxy-Modified Core–Shell MNPs as an Environmentally Friendly and Novel Catalyst for the One-Pot Synthesis of Various Chromene-Annulated Heterocycles, *ACS Omega*, 2021, **6**, 25608–25622.

57 S. Arumugam, N. Senthilkumar, N. Thirumalaivasan, G. Dharman, S. Pandiaraj, M. Rahaman, M. Palaniappan, R. Muthusami, T. Manogaran, L. Mari, K. Kanagaraj, R. Govindasamy and R. Rangappan, Heterogenous copper(II) schiff-base complex immobilized mesoporous silica catalyst for multicomponent biginelli reaction, *J. Organomet. Chem.*, 2023, **998**, 122804.

58 M. Akbari, M. Nikoorazm, B. Tahmasbi and A. Ghorbani-Choghamarani, The new Schiff-base complex of copper(II) grafted on mesoporous KIT-6 as an effective nanostructure catalyst for the homoselective synthesis of various tetrazoles, *Appl. Organomet. Chem.*, 2024, **38**, e7317.

59 B. Tahmasbi, M. Nikoorazm, P. Moradi and Y. A. Tyula, A Schiff base complex of lanthanum on modified MCM-41 as a reusable nanocatalyst in the homoselective synthesis of 5-substituted 1 H-tetrazoles, *RSC Adv.*, 2022, **12**, 34303–34317.

60 Megha, M. Kaur, Diksha, V. Yempally and H. Kaur, Copper(II) Schiff Base Complex Immobilized on Magnetic-Fe3O4 Nanoparticles for Selective Oxidation of Anthracene, *Catal. Lett.*, 2024, **154**, 2606–2619.

61 G. A. Coppola, S. Pillitteri, E. V. Van der Eycken, S.-L. You and U. K. Sharma, Multicomponent reactions and photo/electrochemistry join forces: atom economy meets energy efficiency, *Chem. Soc. Rev.*, 2022, **51**, 2313–2382.

62 H. Farhid, V. Khodkari, M. T. Nazeri, S. Javanbakht and A. Shaabani, Multicomponent reactions as a potent tool for the synthesis of benzodiazepines, *Org. Biomol. Chem.*, 2021, **19**, 3318–3358.

63 P. Das, A. Dutta, A. Bhaumik and C. Mukhopadhyay, Heterogeneous ditopic ZnFe 2 O 4 catalyzed synthesis of 4 H-pyrans: further conversion to 1, 4-DHPs and report of functional group interconversion from amide to ester, *Green Chem.*, 2014, **16**, 1426–1435.

64 S. Gharghish, M. G. Dekamin and S. H. Banakar, Functionalized graphene oxide by 4-amino-3-hydroxy-1-naphthalenesulfonic acid as a heterogeneous nanocatalyst for the one-pot synthesis of tetraketone and tetrahydrobenzo [b] pyran derivatives under green conditions, *Nanoscale Adv.*, 2024, **6**, 3911–3922.

65 S. Momeni and R. Ghorbani-Vaghei, A facile one-pot synthesis of tetrahydrobenzo [b] pyrans and 2-amino-4 H-chromenes under green conditions, *RSC Adv.*, 2024, **14**, 21608–21622.

66 A. M. Delfani, H. Kiyani and M. Zamani, Synthesis of tetrahydrobenzo [b] pyrans catalyzed by 1, 3-dibenzyl-1H-benzo [d] imidazole-3-ium chloride, *Curr. Org. Chem.*, 2023, **27**, 1542–1552.

67 F. Taheri, D. Elhamifar, S. Kargar and A. Zarnegaryan, Magnetic silica supported propylamine/H3PW12O40: A powerful and highly stable nanocatalyst for synthesis of tetrahydrobenzopyrans, *Mater. Chem. Phys.*, 2023, **297**, 127443.

68 P. Gupta, S. Rani, D. Sah, J. Shabir, B. Singh, B. Pani and S. Mozumdar, Basic ionic liquid grafted on magnetic nanoparticles: An efficient and highly active recyclable

catalyst for the synthesis of β-nitroalcohols and 4H-benzo [b] pyrans, *J. Mol. Struct.*, 2023, **1274**, 134351.

69 C. Boureghda, I. Amine Khodja, B. Carboni, R. Boulcina, O. Kermiche and A. Debache, A facile one-pot and green multi-component synthesis of 2-amino-4hpyrans promoted by pyridinium p-toluenesulfonate in aqueous medium, *Lett. Org. Chem.*, 2016, **13**, 482–490.

70 S. Abdolahi, F. Gholamian and M. Hajjami, Preparation and catalytic application of two different nanocatalysts based on hexagonal mesoporous silica (HMS) in synthesis of tetrahydrobenzo [b] pyran and 1, 4-dihydropyrano [2, 3-c] pyrazole derivatives, *Sci. Rep.*, 2022, **12**, 22108.

71 D. Elhamifar, Z. Ramazani, M. Norouzi and R. Mirbagheri, Magnetic iron oxide/phenylsulfonic acid: a novel, efficient and recoverable nanocatalyst for green synthesis of tetrahydrobenzo [b] pyrans under ultrasonic conditions, *J. Colloid Interface Sci.*, 2018, **511**, 392–401.

72 X.-B. Zhang, H.-W. Tong, S.-M. Liu, G.-P. Yong and Y.-F. Guan, An improved Stöber method towards uniform and monodisperse Fe 3 O 4@ C nanospheres, *J. Mater. Chem. A*, 2013, **1**, 7488–7493.

73 S. Sadjadi and N. Bahri-Laleh, CuI@amine-functionalized halloysite as an efficient heterogeneous catalyst for promoting A3 coupling reaction under ultrasonic irradiation: a combination of experimental and DFT simulation, *J. Porous Mater.*, 2018, **25**, 821–833.

74 A. Hendy, N. Hassan, J. El-Nady, A. S. I. Ahmed, R. M. Abou Shahba and T. M. Tamer, Enhancement of biological properties in casein protein through functionalization with cinnamaldehyde via Schiff base bonding: antibacterial and antioxidant effects, *RSC Adv.*, 2025, **15**, 27300–27310.

75 R. H. M. Ali, C.-Y. Hsu, K. M. Thalij, R. H. Althomali, S. Abdullaev, S. F. Abdulameer, A. H. Alawadi, A. Alsaalamy, F. A. Dawood and N. M. Ahmed, An efficient magnetic nanoadsorbent based on functionalized graphene oxide with gellan gum hydrogel embedded with MnFe layered double hydroxide for adsorption of Indigo carmine from water, *Int. J. Biol. Macromol.*, 2023, **253**, 127479.

76 F. Mousavi, D. Elhamifar and S. Kargar, Copper/IL-containing magnetic nanoporous MCM-41: A powerful and highly stable nanocatalyst, *Surf. Interfaces*, 2021, **25**, 101225.

77 E. Brito, D. Gomes, C. P. Cid, J. de Araújo, F. Bohn, L. Streck and J. Fonseca, Superparamagnetic magnetite/IPEC particles, *Colloids Surf., A*, 2019, **560**, 376–383.

78 F. Dadvar and D. Elhamifar, Magnetic silica/graphene oxide nanocomposite supported ionic liquid–manganese complex as a powerful catalyst for the synthesis of tetrahydrobenzopyrans, *Sci. Rep.*, 2023, **13**, 19354.

79 G. M. Ziarani, A. Abbasi, A. Badiei and Z. Aslani, An efficient synthesis of tetrahydrobenzo [b] pyran derivatives using sulfonic acid functionalized silica as an efficient catalyst, *J. Chem.*, 2011, **8**, 293–299.

80 L.-Q. Yu, F. Liu and Q.-D. You, One-pot synthesis of tetrahydrobenzo [b] pyran derivatives catalyzed by amines in aqueous media, *Org. Prep. Proced. Int.*, 2009, **41**, 77–82.

81 K. Taheri, D. Elhamifar, S. Kargar and A. Zarnegaryan, Graphene oxide supported ionic liquid/Fe complex: a robust and highly stable nanocatalyst, *RSC Adv.*, 2023, **13**, 16067–16077.

82 A. Khazaei, F. Gholami, V. Khakyzadeh, A. R. Moosavi-Zare and J. Afsar, Magnetic core–shell titanium dioxide nanoparticles as an efficient catalyst for domino Knoevenagel–Michael-cyclocondensation reaction of malononitrile, various aldehydes and dimedone, *RSC Adv.*, 2015, **5**, 14305–14310.

83 H. R. Saadati-Moshtaghin and F. M. Zonoz, Preparation and characterization of magnetite-dihydrogen phosphate as a novel catalyst in the synthesis of tetrahydrobenzo[b] pyrans, *Mater. Chem. Phys.*, 2017, **199**, 159–165.

84 F. Ataie, D. Abolghasem and A. Khojastehnezhad, Graphene Oxide Functionalized Organic-Inorganic Hybrid (GO–Si–NH2–PMo): An Efficient and Green Catalyst for the Synthesis of Tetrahydrobenzo[b]pyran Derivatives, *Polycyclic Aromat. Compd.*, 2021, **41**, 781–794.

85 M. Salimi, M. A. Nasseri and B. N. Jazi, Cu(II)-immobilized on functionalized magnetic nano-fibrillated cellulose (Fe3O4@NFC/E-CHDA-CuII): a novel, efficient and magnetically nanocatalyst for the one-pot synthesis of tetrahydrobenzo[b]pyran derivatives, *J. Iran. Chem. Soc.*, 2019, **16**, 2221–2230.